



Research article

Potential of bioactive compound of *Cyperus rotundus* L. rhizome extract as inhibitor of PD-L1/PD-1 interaction: An *in silico* study

Wirdatun Nafisah^a, Fatchiyah Fatchiyah^b, Muhammad Hermawan Widyananda^c, Yuyun Ika Christina^a, Muhaimin Rifa'i^b, Nashi Widodo^b, Muhammad Sasmito Djati^{b,*}

^a Doctoral Program, Department of Biology, Faculty of Mathematics and Natural Science, Brawijaya University, Malang, East Java 65145, Indonesia

^b Department of Biology, Faculty of Mathematics and Natural Science, Brawijaya University, Malang, East Java 65145, Indonesia

^c Magister Program, Department of Biology, Faculty of Mathematics and Natural Science, Brawijaya University, Malang, East Java 65145, Indonesia

Article Info

Article history:

Received 17 November 2021

Revised 9 May 2022

Accepted 15 May 2022

Available online 26 August 2022

Keywords:

Cancer,

Cyperus rotundus,

Immune checkpoint,

In silico

Abstract

Importance of the work: The mechanism of cancer escape from immune system elimination is mediated by the PD-L1/PD-1 protein interaction.

Objectives: To investigate the potential of a bioactive compound of *Cyperus rotundus* L. rhizome extract (CRE) as an inhibitor of PD-L1/PD-1 interaction.

Materials & Methods: The plant extraction was carried out using ethanol, and the bioactive compounds of CRE were identified using liquid chromatography-high resolution mass spectrometry. Three CRE bioactive compounds—NCGC00380624-01 (Cmpd1), tetramethylcyclopentadiene (Cmpd2), and luteolin (Cmpd3)—were used for further analysis, consisting of biological activity prediction using the PASS server, molecular docking through Autodock Vina in PyRx and molecular dynamics simulation using the YASARA software. All analyses were compared with BMS-202 as a control inhibitor.

Results: PASS prediction showed several activities of the compounds related to cancer, including the HIF-1 α expression inhibitor. Furthermore, molecular docking analysis showed the potential inhibition of the PD-L1 protein by Cmpd2 and Cmpd3. The inhibition may be attributed to the involvement of key residues between BMS-202 and the PD-L1 protein, such as Tyr56, Ala121, Met115 and Tyr123. The binding energy of BMS-202 was the lowest, followed by Cmpd3, Cmpd2 and Cmpd1 (-11.2 kcal/mol, -8.9 kcal/mol, -6.2 kcal/mol and -4 kcal/mol, respectively). Molecular dynamics simulation confirmed that the most stable interaction was Cmpd3/PD-L1, whereas the most unstable interaction was Cmpd1.

Main finding: The CRE bioactive compounds could be considered as potential inhibitors of PD-L1/PD-1 interaction. This inhibition could be expected to reactivate T cells and enhance their ability to eliminate cancer cells.

* Corresponding author.

E-mail address: msdjati@ub.ac.id (M.S. Djati)

online 2452-316X print 2468-1458/Copyright © 2022. This is an open access article under the CC BY-NC-ND license (<http://creativecommons.org/licenses/by-nc-nd/4.0/>), production and hosting by Kasetsart University of Research and Development Institute on behalf of Kasetsart University.

<https://doi.org/10.34044/j.anres.2022.56.4.09>

Introduction

Globally, there were an estimated 19.3 million new cancer cases and about 10.0 million deaths caused by cancer in 2020, based on the updated GLOBOCAN 2020 data (Sung et al., 2021). Recently, female breast cancer has become the most diagnosed cancer type, followed by lung, colorectal, prostate and stomach cancers (Sung et al., 2021). Cancer is a complex and multifactorial disease, the causes of which can be diverse. Based on Rondeau et al. (2019), there are two tumor formation theories: somatic mutation theory (SMT) and tissue organization field theory (TOFT). The SMT theory explains the formation of the tumor as starting along with genetic mutation in a single cell. However, the appearance of tumors based on the TOFT theory begins from the tumor environment, in which the proliferation of cells and the disruption of tissue architecture lead to mutation.

Gene mutation may cause unregulated and rapid cell proliferation, which is identified as one of cancer's hallmarks and caused by hypoxia, which is found in a solid tumor (Tang et al., 2021). Hypoxia occurs when the oxygen pressure in the tumor microenvironment is lower than 5–10 mmHg that can be caused by two factors: 1) accumulation of oxygen intake due to the high proliferation rate of cells; and 2) insufficient oxygen supply to cells and tissue because of the messy microvasculature tumor tissue and leaky vessels that fail to resolve oxygen deficit (Noman et al., 2019). Hypoxia-inducible factor 1 α (HIF-1 α) is a hypoxia marker and acts as oxygen-dependent regulation that accumulates during hypoxia. Hypoxia induces the expression of PD-L1 in tumor cells through HIF-1 α to support immune escape (Wen et al., 2020). PD-L1 is a ligand of PD-1, a receptor on activated T cells and an immune checkpoint. The overexpression of PD-L1 in tumor cells facilitates immune escape by inhibiting T cells and macrophage phagocytosis (Gordon et al., 2017; Noman et al., 2019). Finding the inhibitor of PD-L1/PD-1 is a promising target in cancer therapy.

Herbal-based therapy is increasingly used as a valuable and effective treatment for cancer because herbal plants are a rich source of phytochemical compounds that play an essential role in developing and discovering new drugs (Hosseini and Ghorbani, 2015). One of the widely used herbal medicine is *Cyperus rotundus* L. or nutgrass. Studies have reported the potential of this plant extract as an anti-cancer agent. For example, as a natural antioxidant source, the rhizome of *C. rotundus* showed a scavenging effect on various types

of free radicals that were found to be a key in anti-cancer activity (Srivastava et al., 2013). It also can induce apoptosis via inhibition of anti-apoptotic protein survivin, Bid, Bcl-2, and induction of Bax, caspase-8 and caspase-9 (Park et al., 2014; Wang et al., 2019). However, although the role of *C. rotundus* in the apoptosis mechanism has been well reported, its contribution remains unclear to enhancing the immune system and the elimination of cancer cells. Therefore, the present study aimed to investigate the potential of bioactive compounds from *C. rotundus* L. rhizome extract (CRE) in inhibiting the PD-L1 immune checkpoint protein which is then expected to enhance the immune system to eliminate cancer cells.

Materials and Methods

Plant material and extraction

The rhizome powder of *C. rotundus* was obtained from UPT. Balai Materia Medika Batu, East Java, Indonesia (7°52'01.2"S; 112°31'13.2"E). Plant determination was identified by UPT Balai Materia Medika with determination number 074/ 536/ 102.7-A/ 2021. The rhizome powder was macerated with ethanol (1:10, mass to volume) and stirred continuously for 24 hr at room temperature. Then, the sample was passed through filter paper and evaporated using a rotary evaporator at 50 °C.

Liquid chromatography-high resolution mass spectrometry analysis

The CRE bioactive compounds were identified using the liquid chromatography-high resolution mass spectrometry (LC-HRMS) analysis method of Christina et al. (2021). The sample was prepared before being injected into LC-HRMS instrument (Thermo Fisher Scientific Inc.; USA) by adding 0.1% ethanol until the final volume was 1,500 μ L. Then, the sample was vortexed at 2,000 revolutions per minute (rpm) for 2 min that was reduced to 6,000 rpm for 2 min. The supernatant was filtered using a 0.22 μ m syringe filter; then, the samples were ready for processing in an autosampler (Thermo Fisher Scientific Inc.; USA).

The LC-HRMS analysis was done by injecting a 100 μ L sample and using solvent A = 0.1% formic acid in water and solvent B = 0.1% formic acid in acetonitrile. The analytical column was a Hypersil GOLD aQ 50 \times 1 mm \times 1.9 μ m particle

size with 40 mL/min analytical flow rate, 30 min of run time and maintained at 30 °C. A Q Exactive™ Orbitrap Mass Spectrometer (MS Thermo Fisher Scientific Inc.; USA) was applied for the detection with a full scan at 70,000 resolution. The Compound Discoverer integrated with mzCloud MS/MS Library software was used to analyze the data (Thermo Fisher Scientific Inc., USA).

Protein-ligand preparation

The CRE bioactive compounds used in this study were: 7,8-bis(hydroxymethyl)-1,4a-dimethyl-3,4,4a,5,6,7-hexahydro-2H-benzo[7]annulen-2-one (Cmpd1), 1,2,3,4-tetramethyl-1,3-cyclopentadiene (Cmpd2) and luteolin (Cmpd3), as shown in Table 1. To compare the inhibition potential of the CRE bioactive compounds, a small molecule inhibitor, BMS-202, was used as a control. The 3D molecular structures of the three bioactive compounds and the control was retrieved from the relevant PubChem chemical databases (<https://pubchem.ncbi.nlm.nih.gov>), which were then minimized for energy and converted into .pdb file format using Open Babel in the PyRx software (Kumar et al., 2021).

Molecular docking was used to evaluate the potential of the CRE bioactive compounds as PD-L1 inhibitor. The PD-L1 protein was obtained from the RSCB protein databank (PDB ID: 5j89; (<https://www.rcsb.org/structure/5J89>)) and was docked against each of the three CRE bioactive compounds and BMS-202 using the Autodock Vina in the PyRx software.

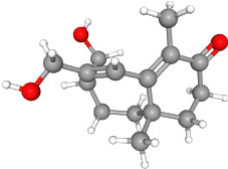
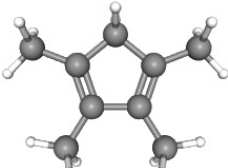
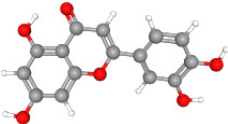
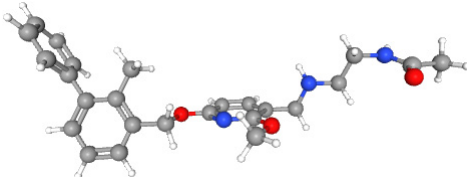
Biological activity prediction

The prediction of biological activity of ligands was carried out using the PASS (Prediction of Activity Spectra for Substances) server (Lagunin et al., 2000). This server predicts the biological activity of over 4,000 kinds, such as the pharmacological, mechanism of action, toxicity and adverse effects. A cut-off value for probable to be active (Pa) of > 0.7) was used to get the highest estimation of the activity of the active compound.

Molecular docking analysis

The docking analysis was performed using Autodock Vina in the PyRx 8.0.0 software (Trott and Olson, 2010) by making

Table 1 Investigated bioactive compounds structure and identification number (CID)

Compound Name	Chemical 3D structure	CID
NCGC00380624-01 (Cmpd1)		45359408
Tetramethylcyclopentadiene (Cmpd2)		138163
Luteolin (Cmpd3)		5280445
BMS-202 (inhibitor)		117951478

Red indicates oxygen atom; blue indicates nitrogen atom

the protein a macromolecule and investigating the bioactive compounds and BMS-202 as ligands. The macromolecule and ligand were docked with the grid setting of centers ($16.4760 \times -18.0355 \times 179.8301$) along with dimension ($21.0270 \text{ \AA} \times 14.0155 \text{ \AA} \times 19.2147 \text{ \AA}$). The docking outcomes were visualized using the Discovery Studio 2016 software (Haque et al., 2022).

Molecular dynamic simulation

Molecular dynamic simulations were carried out using the YASARA software (Krieger and Vriend, 2015). The cells were set in a cube shape with the lengths of the X, Y, and Z axes, ($115,657, 115,657, 115,657 \text{ \AA}$; 20 \AA larger than the protein). The cell was filled with water as a solvent with 0.997 g/mL density. Environmental parameters were regulated as cell physiological conditions (37°C , 1 atmosphere, pH 7.4, 0.9% salt content) using a Berendsen thermostat (298 K) and barostat (1 pressure bar), according to Bahun et al. (2022) for 40 ns with autosave every 25 ps. The simulations were performed using the AMBER14 force field. The macro md_run program was used for running simulations. The macro MD analysis program was used to analyze the root-mean-square deviation (RMSD), the radius of gyration and the number of hydrogen bonds. The root mean square fluctuation (RMSF) and molecular dynamic binding energy were analyzed using macro md_analyzeres and md_analyzebindenergy, respectively.

Results

Liquid chromatography-high resolution mass spectrometry analysis

The raw data from the LC-HRMS and single chromatogram were processed using the Mzmine 2 software integrated with the mzCloud MS/MS Library. At least three bioactive compounds were contained in the CRE: NCGC00380624-01 (Cmpd1), tetramethylcyclopentadiene (Cmpd2) and luteolin (Cmpd3). The retention times (RTs) and m/z values of the compound's the single chromatogram for each compound are presented in Fig. 1 and Fig. 2, respectively. The retention times for Cmpd1, Cmpd2 and Cmpd3 were 0.914 min, 17.821 min and 0.896 min, respectively, and their m/z values were 251.16422, 123.11694, and 287.05499, respectively.

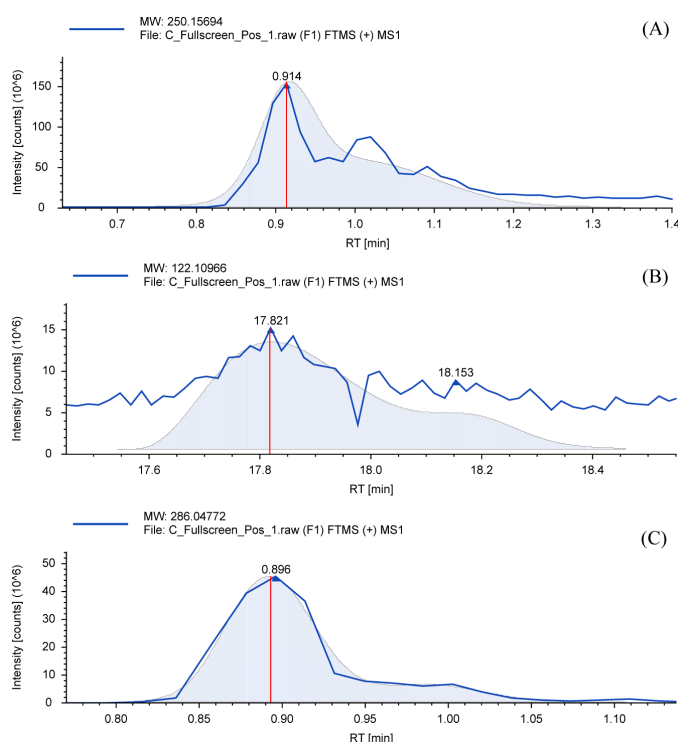


Fig. 1 Single chromatogram of compounds from *Cyperus rotundus* L. rhizome extract showing retention time (RT) and molecular weight (MW). (A) Cmpd1; (B) Cmpd2; and (C) Cmpd3

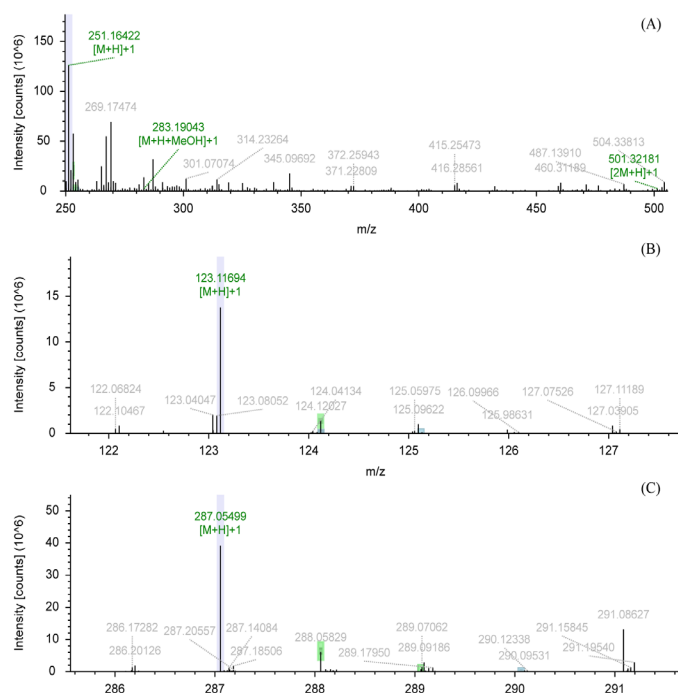


Fig. 2 Identified compounds in *Cyperus rotundus* L. rhizome extract at different retention times: (A) 0.914 min; (B) 17.821 min; (C) 0.896 min, where blue highlight indicates the monoisotopic mass expected compound ion and green highlight indicates delta mass and relative intensity of isotope pattern.

Biological activity prediction

Based on the PASS server analysis, several biological activities related to cancer were identified in the investigated bioactive compounds (Table 2). Cmpd1 showed apoptosis agonist and anti-inflammatory activity with Pa values of 0.795 and 0.739, respectively. Anti-inflammatory activity was also predicted in Cmpd2 (Pa = 0.799), along with HIF1 α expression inhibitor, BRAF expression inhibitor and JAK2 expression inhibitor with Pa values of 0.788, 0.762, and 0.730, respectively. Cmpd3 had a high Pa value compared to Cmpd1 and Cmpd2 with the biological activities, such as HIF1 α expression inhibitor (Pa = 0.964), TP53 expression enhancer (0.916), apoptosis agonist (0.866), JAK2 expression inhibitor (0.833) and MMP9 expression inhibitor (0.777). Inhibitors with very low Pa values (< 0.3) were antineoplastic (small cell lung cancer; Pa = 0.221), antineoplastic (bone cancer; Pa = 0.203), transcription factor STAT3 inhibitor (Pa = 0.186) and MAP kinase 9 inhibitor (Pa = 0.061).

Molecular docking analysis

Based on the molecular docking analysis, BMS-202 binds to PD-L1 via several amino acid residues (Tyr123,

Arg125, Ala121) as hydrogen bond interaction and Ala121, Met115, Tyr56 as hydrophobic interaction (Table 3, Fig. 3). The residue involved in the BMS-202 interaction was considered as the key that was essential in the inhibition of the PD-L1 protein. The binding energy of BMS-202/PD-L1 had the lowest energy, followed by Cmpd3, Cmpd2 and Cmpd1 (-11.2, -8.9, -6.2, and -4 kcal/mol, respectively). As shown in Table 3, Cmpd3 had the lowest binding energy compared to other CRE compounds and interacted with four hydrogen bonds (to Tyr56, Gln66, Asp122 and Ile116). Cmpd3 also bound to PD-L1 via electrostatic interaction involving Asp122 residue and hydrophobic interaction involving residues Ala121 and Met15. The involvement of the Tyr56, Ala121 and Met115 key residues showed the inhibition potential of Cmpd3 against the PD-L1 protein. Furthermore, Cmpd2 showed inhibition potential against the PD-L1 protein due to the involvement of the key residues Ala121, Tyr123, Tyr56 and Met115 through hydrophobic interactions. Unfortunately, the interaction was weaker than Cmpd3, as indicated by no hydrogen bond interaction and the higher binding energy (-6.2 kcal/mol). Furthermore, Cmpd1 had a low inhibition potential against the PD-L1 protein, demonstrated by its highest binding energy and no key residue involvement (Table 3).

Table 2 Biological activity prediction

Compound	Biological activity	Pa	Pi
Cmpd1	Apoptosis agonist	0.795	0.008
	Anti-inflammatory	0.739	0.011
Cmpd2	Anti-inflammatory	0.799	0.007
	HIF1 α expression inhibitor	0.788	0.013
	BRAF expression inhibitor	0.762	0.002
	JAK2 expression inhibitor	0.730	0.014
Cmpd3	HIF1 α expression inhibitor	0.964	0.003
	TP53 expression enhancer	0.916	0.004
	Apoptosis agonist	0.866	0.005
	JAK2 expression inhibitor	0.833	0.006
	MMP9 expression inhibitor	0.777	0.004
BMS-202	Antineoplastic (small cell lung cancer)	0.221	0.142
	Antineoplastic (bone cancer)	0.203	0.145
	Transcription factor STAT3 inhibitor	0.186	0.146
	MAP kinase 9 inhibitor	0.061	0.036

Pa = Probable to be active; Pi = Probable to be inactive

Table 3 Binding energy and residue of ligand-PD-L1 protein interaction

No	Ligand	Residues	Interaction	Binding energy (kcal/mol)
1	BMS-202	Tyr123, Arg125, Ala121 Ala121, Met115, Tyr56	Hydrogen bond (3) Hydrophobic (5)	-11.2
1	Cmpd1	Ile54, Val68 Phe19, Ala18	Hydrophobic (2) Unfavorable bond (2)	-4
2	Cmpd2	Ala121, Ile24, Tyr123, Tyr56, Met115	Hydrophobic (7)	-6.2
3	Cmpd3	Tyr56, Gln66, Asp122, Ile116 Asp122 Ala121, Met115 Met115	Hydrogen bond (4) Electrostatic (1) Hydrophobic (3) Other (1)	-8.9

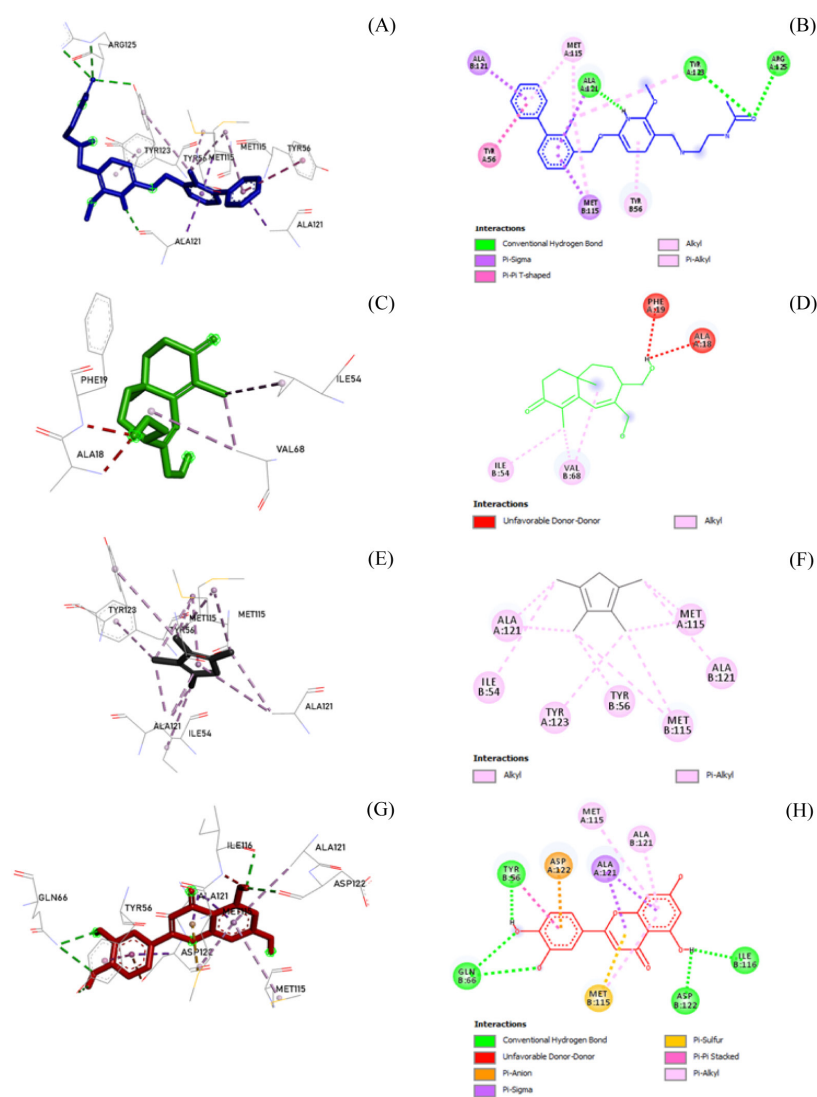


Fig. 3 Interactions of BMS-202 and *Cyperus rotundus* L. rhizome extract bioactive compounds against PD-L1 protein (A; C; E; G). 3D model of ligand interaction with interacting protein atom (B; D; F; H), where 2D diagram of ligand interaction in A and B is for BMS-202, in C and D is for Cmpd1, in E and F is for Cmpd2 and in G and H is for Cmpd3

Molecular dynamic simulation

Molecular dynamic simulation was carried out to analyze the stability of the interactions between PD-L1 and BMS-202, Cmpd1, Cmpd2 and Cmpd3. The simulation showed that the PD-L1 conformation tended to be stable when interacting with the three compounds seen from the RMSD backbone, which was always below 3 Å and had minimal fluctuations (Fig. 4A). The RMSD result was supported by the hydrogen bonds and the RMSF value. The number of hydrogen bonds in the protein-BMS-202 and in the protein-Cmpd1, 2, and 3 complexes were not much different. The number of hydrogen bonds between the proteins and water was not much different in all complexes (Figs. 4E and 4F). The RMSF values were not much different in all complexes (Fig. 5). The radius of gyration also indicated that the protein remained in a compact and stable state (Fig. 4G). The ligand structure was also stable during the simulation, with minimal fluctuations from the RMSD ligand conformation value (Fig. 4D).

The stability of the interaction of PD-L1 with the ligand can be analyzed from the results of molecular dynamics simulations. The RMSD complex values indicated that the interactions between PD-L1 and Cmpd2 and Cmpd3 tended to be stable. However, the interaction of PD-L1 with Cmpd1 was unstable, characterized by the big drift and very high complex RMSD values ranging from ~36 ns until the end of the simulation (Fig. 4B). The RMSD ligand movement value of Cmpd1 was also very high, being even greater than 10 Å at ~36 ns, indicating that Cmpd1 had been released from the protein (Fig. 4C), which was confirmed by the visualization of the final molecular dynamics simulation compared to its before state (Fig. 6C). Otherwise, this visualization showed BMS-202, Cmpd2 and Cmpd3 remained in the same binding pocket as those from docking (or before molecular dynamics

simulation at 0 ns) and in the final interaction after molecular dynamics simulation (40 ns), as shown in Figs. 6A, 6C and 6D. Molecular dynamic binding energy showed that BMS-202 and Cmpd3 bound to protein stably, characterized by positive values and minimal fluctuations. In contrast, Cmpd1 and Cmpd2 tended to be unstable because they had low molecular dynamic binding energies and a lot of fluctuation (Fig. 4H).

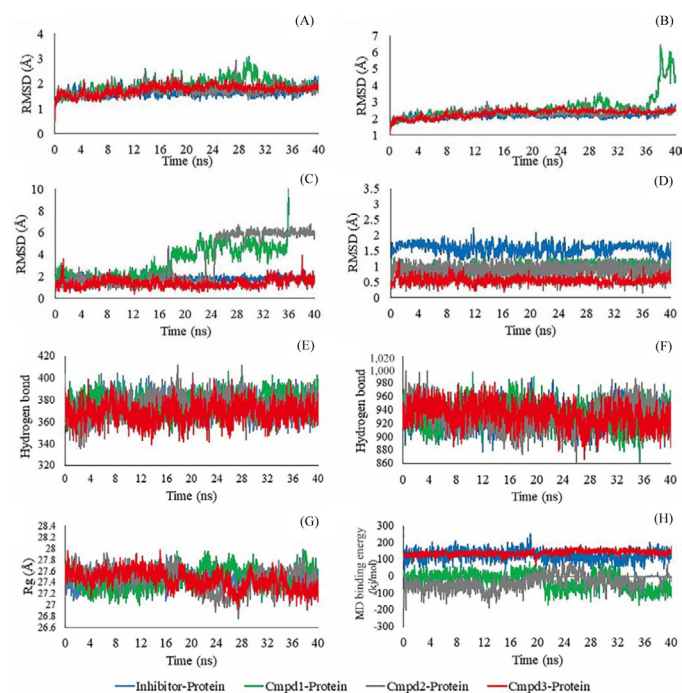


Fig. 4 Molecular dynamic simulation results: (A) root-mean-square deviation (RMSD) backbone protein; (B) complex protein-ligand RMSD; (C) RMSD ligand movement; (D) RMSD ligand conformation; (E) number of protein hydrogen bonds during simulation; (F) number of protein-water hydrogen bonds during simulation; (G) radius of gyration (Rg) protein-ligand complex; (H) molecular dynamic binding energy (MD)

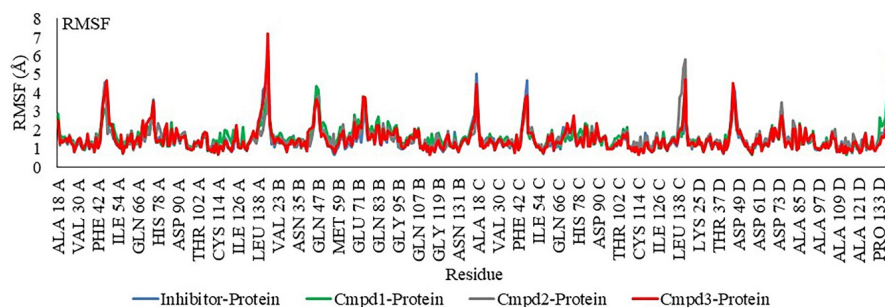


Fig. 5 Molecular dynamic result of root mean square fluctuation (RMSF)

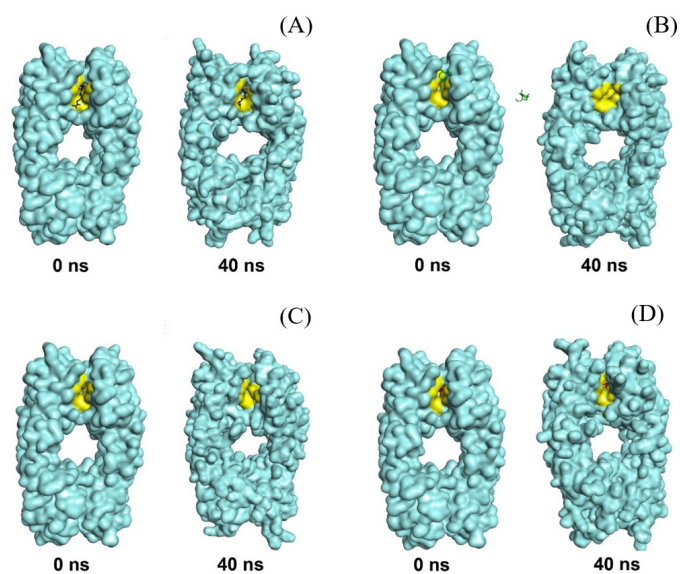


Fig. 6 Ligand position and binding pocket visualization (yellow), before (0 ns) and after (40 ns) molecular dynamics simulation for: (A) BMS-202; (B) Cmpd1; (C) Cmpd2; (D) Cmpd3

After molecular dynamics simulation, the interaction of BMS-202 and the CRE bioactive compounds against the PD-L1 protein were visualized to evaluate the involvement of the residues after being exposed to a dynamic condition in molecular dynamics. The visualization is shown in a 2D diagram (Fig. 7). Compared to docking, the residue involvement was similar in the interaction of the ligand-protein complex after molecular dynamics simulation. There was only one residue addition or change in all the complexes, that being for the Cmpd1 and PD-L1 protein interaction. Since Cmpd1 was detached from the protein after molecular dynamics simulation (Fig. 6B), there was no PD-L1 protein residue interaction with Cmpd1 (Fig. 7B). The environments of the BMS-202, Cmpd2 and Cmpd3 interactions against PD-L1 were also similar to those in docking. The hydrogen bond and hydrophobic interaction still occurred in BMS-202 and Cmpd3 against the PD-L1 protein (Figs. 7A and 7D) and hydrophobic interaction was also found in the interaction involving Cmpd2 and PD- interaction after the simulation (Fig. 7C). The results of this molecular dynamics simulation suggested that the most stable compound interacting with PD-L1 was Cmpd3, while the least stable was Cmpd1.

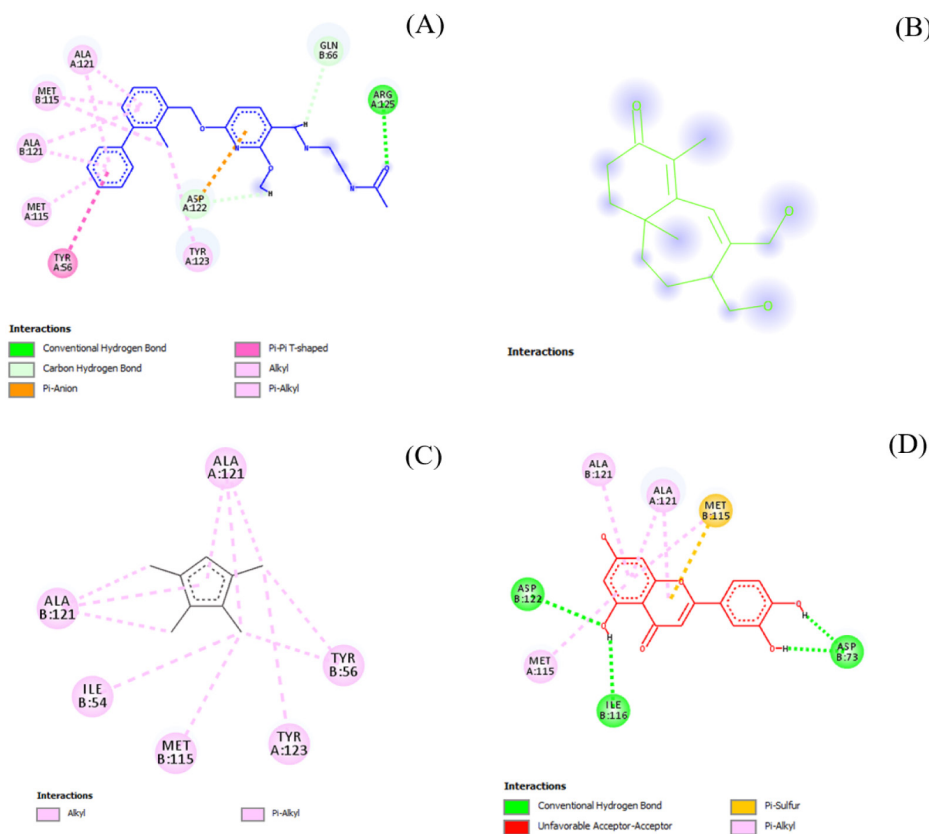


Fig. 7 2D diagrams of interaction of BMS-202 and bioactive compounds of *Cyperus rotundus* L. rhizome extract against PD-L1 protein after molecular dynamics simulation: (A) BMS-202; (B) Cmpd1 (no interaction); (C) Cmpd2; (D) Cmpd3

Discussion

Cancer cells can avoid immune elimination via an immune escape mechanism, which is one of the significant challenges in cancer therapy. There are “brakes” on the immune function, such as the immune checkpoint of PD-1 and cytotoxic T-lymphocyte-associated protein 4 (CTLA-4) that is associated with the inhibition of its immune checkpoint. Finding the inhibitor may be important in T cell reactivation and is expected to enhance the elimination of cancer cells (Han et al., 2020). Therefore, the development of PD-L1/PD-1 immune checkpoint inhibitors has become a target for therapeutic strategies.

This study aimed to find the potential inhibitor of CRE bioactive compounds against the PD-L1 immune checkpoint using molecular docking and molecular dynamics simulation. Prior to this the biological activity was analyzed of the investigated bioactive compounds using PASS server. Several cancer-related activities were found; however, only one activity (the HIF-1 α expression inhibitor) was indirectly correlated with the immune checkpoint mechanism. HIF1- α is a protein that plays a role in stimulating PD-L1 transcription by binding HIF-1 α to the PD-L1 promoter, the hypoxia response element (Wang et al., 2018). So, inhibiting the expression of HIF-1 α may lead to the inhibition of PD-L1 expression. Based on the PASS analysis, Cmpd2 and Cmpd3 showed activity of the HIF-1 α expression inhibitor and were expected to inhibit the PD-L1 protein, which would subsequently reactivate T cell activity.

Based on molecular docking, the results identified the potential inhibition of CRE bioactive compounds against the PD-L1 protein, such as Cmpd2 (tetramethylcyclopentadiene) and Cmpd3 (luteolin). The inhibitory potential of the compounds was shown by the involvement of key residues of the BMS-202/PD-L1 interaction, such as Tyr56, Ala121, Met115 and Tyr123. BMS-202 was used as a control inhibitor due to its function in ruining PD-L1 recognition by PD-1 *in vitro*. BMS-202 can inhibit PD-L1 by inducing two free soluble PD-L1 dimerizations via PD-L1/PD-1 binding epitopes, known as the dimer-locking mechanism (Ganesan et al., 2019). In addition, Ganesan et al. (2019) stated that the interaction of BMS small molecule against the PD-L1 protein that formed hydrogen bond interactions via Asp122 and Gln66 could stabilize this complex. This finding supported the interaction of Cmpd3 against residue Asp122 of PD-L1 via electrostatic interaction being expected to stabilize this binding. BMS-8 and BMS-1166 also induced PD-L1 dimerization by involving Ile54, Tyr56, Met155, Ala121 and Tyr123, which stabilized their binding through non-polar interaction (Shi et al., 2019). The hydrogen bond is an essential type of bonding

used to determine the shape and function of biomolecules, as well as playing a critical role in enzymatic catalysis to stabilize a ligand in a binding pocket (Kostal, 2016). As shown in Table 3, the Cmpd3/PD-L1 complex has four hydrogen bonds, the highest number compared to the other investigated complexes, including BMS-202/PD-L1, which only has three hydrogen bonds. The large number of hydrogen bonds formed is expected to strengthen the complex of Cmpd3 against PD-L1 protein.

This study used molecular dynamics simulation to confirm the stabilization of the ligand-protein interaction. Molecular dynamics simulation is used to analyze the stability of protein-ligand interactions in specific environments. The stability of this interaction was represented by the RMSD value. A complex is declared stable if it has a low RMSD value and minimal fluctuation (Ghosh et al., 2021). A low RMSD value and minimal fluctuation also shows the stability of the ligand when interacting with the protein (Tou et al., 2013). An RMSD value of more than 3 Å represents a complex structure undergoing a conformational change, indicating instability (Martinez, 2015). The RMSD ligand conformation value represents the stability of the ligand when it interacts with the protein. Molecular dynamics binding energy was also used to estimate the stability of protein-ligand interactions. The more positive the molecular dynamic binding energy value, the more stable the protein-ligand interaction (Chen et al., 2015). The present study found that Cmpd3 had a low RMSD value (< 3 Å) of the backbone protein, protein-ligand complex, ligand movement and ligand conformation, which indicated it was the most stable interaction compared to the other complexes. The stability of the Cmpd3/PD-L1 protein was also supported it having the highest value of the binding energy of the complexes. Based on the molecular dynamics simulation results, the binding pocket position and residues involved in the interaction of the Cmpd3/PD-L1 complex also confirmed its stability. Cmpd3 stayed in the binding pocket of the PD-L1 inhibition sites and involved the key residues in protein inhibition even after molecular dynamics. This result strengthened the prediction of the current study that Cmpd3 had high inhibitory potential against the PD-L1 protein since the molecular docking and dynamic simulation results were complementary.

The ethanol extract of *C. rotundus* L. has high potential to inhibit the PD-L1/PD-1 protein interaction which would then be expected to reactivate T cells and enhance its ability to eliminate cancer cells. These findings suggest an approach for better utilization of the phytochemical compounds of *C. rotundus* L. in the treatment of breast cancer. More methodological research on the isolation of single compounds and *in vivo* investigation is needed to develop an effective therapeutic approach against breast cancer.

Conflict of Interest

The authors declare that there are no conflicts of interest.

Acknowledgements

The Directorate of Research and Community Service funded this research through Program Magister menuju Doktor Sarjana Unggul (PMDSU) (grant no. 993.6/UN10.C10/PN/2020).

References

- Bahun, M., Jukić, M., Oblak, D., et al. 2022. Inhibition of the SARS-CoV-2 3CLpro main protease by plant polyphenols. *Food Chem.* 373: 131594. doi.org/10.1016/j.foodchem.2021.131594
- Chen, D.E., Willick, D.L., Ruckel, J.B., Floriano, W.B. 2015. Principal component analysis of binding energies for single-point mutants of hT2R16 bound to an agonist correlate with experimental mutant cell response. *J. Comput. Biol.* 22: 37–53. doi.org/10.1089/cmb.2014.0192
- Christina, Y.I., Nafisah, W., Atho'illah, M.F., Rifa'i, M., Widodo, N., Djati, M.S. 2021. Anti-breast cancer potential activity of *Phaleria macrocarpa* (Scheff.) Boerl. leaf extract through *in silico* studies. *J. Pharm. Pharmacogn. Res.* 9: 824–845.
- Ganesan, A., Ahmed, M., Okoye, I., et al. 2019. Comprehensive *in vitro* characterization of PD-L1 small molecule inhibitors. *Sci. Rep.* 9: 12392. doi.org/10.1038/s41598-019-48826-6
- Ghosh, R., Chakraborty, A., Biswas, A., Chowdhuri, S. 2021. Identification of polyphenols from *Broussonetia papyrifera* as SARS CoV-2 main protease inhibitors using *in silico* docking and molecular dynamics simulation approaches. *J. Biomol. Struct. Dyn.* 39: 6747–6760. doi.org/10.1080/07391102.2020.1802347
- Gordon, S.R., Maute, R.L., Dulken, B.W., et al. 2017. PD-1 expression by tumour-associated macrophages inhibits phagocytosis and tumour immunity. *Nature* 545: 495–499. doi.org/10.1038/nature22396
- Han, Y., Liu, D., Li, L. 2020. PD-1/PD-L1 pathway: Current researches in cancer. *Am. J. Cancer Res.* 10: 727–742
- Haque, A., Baig, G.A., Alshawli, A.S., et al. 2022. Interaction analysis of MRP1 with anticancer drugs used in ovarian cancer: *In silico* approach. *Life* 12: 383.
- Hosseini, A., Ghorbani, A. 2015. Cancer therapy with phytochemicals: Evidence from clinical studies. *Avicenna J. Phytomed.* 5: 84–97.
- Krieger, E., Vriend, G. 2015. New ways to boost molecular dynamics simulations. *J. Comput. Chem.* 36: 996–1007. doi.org/10.1002/jcc.23899
- Kostal, J. 2016. Computational chemistry in predictive toxicology: Status quo et quo vadis?. *Adv. Mol. Toxicol.* 10: 139–186. doi.org/10.1016/B978-0-12-804700-2.00004-0
- Kumar, G.S., Manivannan, R., Nivetha, B. 2021. *In silico* identification of flavonoids from *Coriandrum sativum* seeds against coronavirus Covid-19 main protease. *J. Drug Deliv. Ther.* 11: 145–152.
- Lagunin, A., Stepanchikova, A., Filimonov, D. Poroikov, V. 2000. PASS: Prediction of activity spectra for biologically active substances. *Bioinformatics* 16: 747–748. doi.org/10.1093/bioinformatics/16.8.747
- Martinez, L. 2015. Automatic identification of mobile and rigid substructures in molecular dynamics simulations and fractional structural fluctuation analysis. *PLoS One* 10: e0119264. doi.org/10.1371/journal.pone.0119264
- Noman, M.Z., Hasmim, M., Lequeux, A., Xiao, M., Duhem, C., Chouaib, S., Berchem, G. Janji, B. 2019. Improving cancer immunotherapy by targeting the hypoxic tumor microenvironment: New opportunities and challenges. *Cells* 8: 1083. doi.org/10.3390/cells8091083
- Park, S.E., Shin, W.T., Park, C., et al. 2014. Induction of apoptosis in MDA-MB-231 human breast carcinoma cells with an ethanol extract of *Cyperus rotundus* L. by activating caspases. *Oncol. Rep.* 32: 2461–2470. doi.org/10.3892/or.2014.3507
- Rondeau, E., Larmonier, N., Pradeu, T. Bikfalvi, A. 2019. Philosophy of biology: Characterizing causality in cancer. *eLife* 8: e53755. doi.org/10.7554/eLife.53755
- Shi, D., An, X., Bai, Q., Bing, Z., Zhou, S., Liu, H. Yao, X. 2019. Computational insight into the small molecule intervening PD-L1 dimerization and the potential structure-activity relationship. *Front. Chem.* 7: 764. doi.org/10.3389/fchem.2019.00764
- Srivastava, R.K., Singh, A. Shukla, S.V. 2013. Chemical investigation and pharmaceutical action of *Cyperus rotundus*—A review. *J. Biol. Act. Prod. Nat.* 3: 166–172. doi.org/10.1080/22311866.2013.833381
- Sung, H., Ferlay, J., Siegel, R.L., Laversanne, M., Soerjomataram, I., Jemal, A., Bray, F. 2021. Global cancer statistics 2020: GLOBOCAN estimates of incidence and mortality worldwide for 36 cancers in 185 countries. *CA-Cancer J. Clin.* 71: 209–249. doi.org/10.3322/caac.21660
- Tang, M., Bolderson, E., O'Byrne, K.J. Richard, D.J. 2021. Tumor hypoxia drives genomic instability. *Front. Cell Dev. Biol.* 9: 626229. doi: 10.3389/fcell.2021.626229
- Tou, W.L., Chang, S.S., Lee, C.C., Chen, Y.C. 2013. Drug design for neuropathic pain regulation from traditional Chinese medicine. *Sci. Rep.* 3: 844. doi.org/10.1038/srep00844
- Trott, O., Olson, A.J. 2010. AutoDock Vina: Improving the speed and accuracy of docking with a new scoring function, efficient optimization, and multithreading. *J. Comput. Chem.* 31: 455–461. doi: 10.1002/jcc.21334
- Wang, F., Song, X., Ma, S., et al. 2019. The treatment role of *Cyperus rotundus* L. to triple-negative breast cancer cells. *Biosci. Rep.* 39: BSR20190502. doi: 10.1042/BSR20190502
- Wang, Y., Wang, H., Yao, H., Li, C., Fang, J.Y., Xu, J. 2018. Regulation of PD-L1: Emerging routes for targeting tumor immune evasion. *Front. Pharmacol.* 9: 536. doi.org/10.3389/fphar.2018.00536
- Wen, Q., Han, T., Wang, Z., Jiang, S. 2020. Role and mechanism of programmed death-ligand 1 in hypoxia-induced liver cancer immune escape (review). *Oncol. Lett.* 19: 2595–2601. doi.org/10.3892/ol.2020.11369